The Astronomical Journal, 163:178 (16pp), 2022 April https://doi.org/10.3847/1538-3881/ac52f6

The Solar Neighborhood. XLIX. New Discoveries and Orbits of M-dwarf Multiples with Speckle Interferometry at SOAR

Eliot Halley Vrijmoet[1,2,6], Andrei Tokovinin[3], Todd J. Henry[2,6], Jennifer G. Winters[4,6], Elliott Horch[5], and Wei-Chun Jao[1,6]
[1] Department of Physics and Astronomy, Georgia State University, Atlanta, GA 30303, USA; vrijmoet@astro.gsu.edu
[2] RECONS Institute, Chambersburg, PA 17201, USA
[3] Cerro Tololo Inter-American Observatory | NSF's NOIRLab, Casilla 603, La Serena, Chile
[4] Center for Astrophysics | Harvard & Smithsonian, 60 Garden Street, Cambridge, MA 02138, USA
[5] Department of Physics, Southern Connecticut State University, 501 Crescent Street, New Haven, CT 06515, USA
Received 2021 November 13; revised 2022 January 14; accepted 2022 February 3; published 2022 March 18

Abstract

We present the first results of a multiyear program to map the orbits of M-dwarf multiples within 25 pc. The observations were conducted primarily during 2019–2020 using speckle interferometry at the Southern Astrophysical Research Telescope in Chile, using the High-Resolution Camera mounted on the adaptive optics module (HRCam+SAM). The sample of nearby M dwarfs is drawn from three sources: multiples from the RECONS long-term astrometric monitoring program at the SMARTS 0.9 m; known multiples, for which these new observations will enable or improve orbit fits; and candidate multiples flagged by their astrometric fits in Gaia Data Release 2 (DR2). We surveyed 333 of our 338 M dwarfs via 830 speckle observations, detecting companions for 63% of the stars. Most notably, this includes new companions for 76% of the subset selected from Gaia DR2. In all, we report the first direct detections of 97 new stellar companions to the observed M dwarfs. Here we present the properties of those detections, the limits of each nondetection, and five orbits with periods 0.67–29 yr already observed as part of this program. Companions detected have projected separations of 0.″024–2.″0 (0.25–66 au) from their primaries and have $\Delta I \lesssim 5.0$ mag. This multiyear campaign will ultimately map complete orbits for nearby M dwarfs with periods up to 3 yr, and provide key epochs to stretch orbital determinations for binaries to 30 yr.

Unified Astronomy Thesaurus concepts: Speckle interferometry (1552); Binary stars (154); Astrometric binary stars (79); Astrometry (80); M stars (985); Low mass stars (2050)

Supporting material: machine-readable tables

1. Introduction

Stars in binary and multiple star systems have been observed in many varieties of orbits, each the result of the stellar formation and dynamical evolution processes that guided them through to the present day. Multiples may form from fragmentation at overdensities in the collapsing molecular cloud (Pringle 1989), creating gravitationally bound stars separated by thousands of astronomical units (Offner et al. 2016; Kuffmeier et al. 2019; Lee et al. 2019), or may form later from the fragmentation of the disk around a (single) protostar, generating stars separated by 50–200 au (Bonnell & Bate 1994; Kratter et al. 2010). Observers, however, have noted a wealth of systems with separations of $\lesssim$10 au, indicating that many of these multiples undergo significant dissipative processes to lose their angular momentum (Duchêne & Kraus 2013). As reviewed in Bate (2015) and Lee et al. (2020), such processes could involve close encounters with nearby stellar neighbors or interactions with the circumstellar or circumbinary disk(s), such as accretion, which in turn is affected by magnetic field interactions and metallicity (Moe et al. 2019).

Clarifying the roles of these processes requires detailed numerical models and, above all, observed distributions of the orbital parameters such as orbital period, semimajor axis, eccentricity, and mass ratio, that are affected by these dissipative processes. For example, a distribution favoring high eccentricities suggests a thermal distribution of orbital velocities produced by dominating dynamical interactions (Kroupa 2008), and has been observed for systems with early-type primary stars (Moe & Di Stefano 2017). Or, as a broader example, if the presence of a disk generally dampens eccentricity, then any trends of eccentricity with semimajor axis could be linked to disk size scales. Key information will come especially from the inclusion of higher-order multiples such as triples and quadruples, rather than binaries alone, as those systems carry additional evidence through their ratios of masses and orbital periods and the mutual inclinations of their orbits.

Previous efforts establishing orbital element distributions for main sequence multiples have focused on specific spectral type or mass regimes. For example, binaries of solar-type stars of types FGK were the focus of Duquennoy & Mayor (1991) and a succeeding effort by Raghavan et al. (2010). Results for early-type binaries with O primary stars were presented by Mason et al. (1998), with additional analysis that compared the O and B massive stars to the solar-type stars by Moe & Di Stefano (2017). Each of these efforts has discussed the observed distribution of eccentricity as a function of orbital period ($P_{\rm orb}$ versus e), highlighting that solar-type and more

[6] Visiting Astronomer, Cerro Tololo Inter-American Observatory. CTIO is operated by AURA, Inc., under contract to the National Science Foundation.

massive systems show a clear correlation between period and eccentricity, with the shortest-period systems almost exclusively circular. In contrast, the very-low-mass systems ($\lesssim 0.1\,M_{\odot}$) presented by Dupuy & Liu (2017) did not show this correlation. This result suggests a mass-dependent or age-dependent difference in dynamical histories or formation pathways of stellar multiples.

M dwarfs make up ∼75% of all stars (Henry et al. 2006, 2018), and a detailed study of their orbital architectures would complete the sweep of stars along the main sequence. With masses spanning 0.08–0.62 $M_{\odot}$ (Benedict et al. 2016), they are the primary product of the star formation process, so their ubiquity renders their orbital parameter distributions of particular interest. In an initial effort, M-dwarf systems showed a solar-type $P_{\rm orb}$ versus e distribution in Udry et al. (2000), but their results were limited by their small sample of 48 systems, and an expanded sample is needed.

To bolster the statistics for M-dwarf multiples, we are assembling a sample of at least 120 M-dwarf systems with accurately measured orbits spanning periods 0–30 yr and semimajor axes up to ∼10 au (depending on stellar mass). This sample size makes this study the largest on M-dwarf multiples' orbits to date. With a particular focus on orbital eccentricity, our goals include determining the period at which tidal circularization occurs and to reveal any structures in the $P_{\rm orb}$ versus e diagram. Our specific goal is to determine 120 orbits in an attempt to populate the final $P_{\rm orb}$ versus e plot with roughly 20 orbits in each 5 yr bin of $P_{\rm orb}$, making the eccentricity distributions clear overall as well as within each of those regimes. The specific goal of 120 orbits has been set to maximize the detail of the final distribution with consideration for availability of resources. We are collecting these orbits from broader sets of multiples observed in the long-term RECONS (REsearch Consortium On Nearby Stars; www.recons.org) astrometry program (as described in Vrijmoet et al. 2020), known orbits in the literature (including the ∼30 published from the Udry et al. (2000) sample described above, and a new multi-epoch speckle interferometry campaign.

This paper presents the first results of the speckle observations, which are being carried out at the Southern Astrophysical Research (SOAR) 4.3 m telescope in Chile using the High-Resolution Camera (HRCam) and SOAR Adaptive Optics Module (SAM; Tokovinin 2018b). This productive telescope-instrument combination has been used to derive hundreds of high-quality orbits over the past decade (e.g., Tokovinin et al. 2019, 2020). Observations for this M-dwarf project have progressed at a rapid pace since commencing in 2019, with orbital motion clearly visible already for several targets. The resulting characterization of M-dwarf multiples, in parallel with our complementary multiplicity study of K dwarfs (Henry et al. 2021), will provide key comparisons between the lowest-mass stars and their higher-mass cousins, as well as a data set well-suited to constraining formation and dynamical evolution models of multistar systems. In this paper, we focus on the M dwarfs, describing the sample in Section 2, the speckle observations in Section 3, and results of the SOAR effort in Section 4. Discussion of the results proceeds in Section 5.

2. Sample

The targets in this program are 338 known and candidate M-dwarf multiples within 25 pc visible from the Southern Hemisphere. By the end of 2020, 333 of these targets have been observed at SOAR.

Distances were determined via parallaxes from the RECONS astrometry program at the SMARTS 0.9 m (Section 2.1 in this paper; also Jao et al. 2005; Henry et al. 2018) and Gaia DR2 (Gaia Collaboration et al. 2016, 2018); all systems meet the 25 pc cutoff in one or both of these catalogs.[7] The full sample will be volume-limited, but does not need to be volume-complete. M dwarfs have been selected as having $V-K_s>3.70$ using Johnson V and 2MASS K_s (hereafter K) filters, as well as absolute magnitude $M_V>9.02$. These limits were established as the M_V and M_K values corresponding to 0.6 $M_{\odot}$ using the Benedict et al. (2016) mass–luminosity relation for M dwarfs. This sample thus spans spectral types M0 through M9. For 11 systems that had no V measurements available, we converted the Gaia DR2 B_G and R_G magnitudes to V using the relations for M dwarfs in Jao et al. (2018). Finally, the specifications of HRCam+SAM on SOAR limit the sample to systems brighter than $I=14$ mag and south of +25° in decl.

The primary goal of the project is to map the distribution of orbital eccentricity with respect to orbital period, with the sample of 338 systems intended to support an even representation of periods 0–30 yr. Although determining 120 accurate orbits is the primary goal, the speckle sample includes several times that many systems; this reflects our expectation that only a subset will have well-defined orbits with $P_{\rm orb}<30$ yr by the end of the 3 yr observing campaign. To reach 120 orbits, the full project sample will include orbits observed using additional methods from other programs with a variety of time baselines and strengths, e.g., long-term astrometry and systems with spectroscopic orbits. Because this paper presents results of the speckle subset only, hereafter the "sample" and similar terms will refer to the speckle subsample rather than the ultimate full project sample that will include all observing methods.

Table 1 lists the entire speckle sample of 338 M dwarfs targeted at SOAR, including the five stars not yet observed by the end of 2020. For each target are listed R.A. and decl. 2000.0 positions (columns 1–2), the WDS-style coordinate name (column 3), the WDS discoverer code if the pair has been previously resolved (column 4), and the target name used in other RECONS work (column 5). These identifying parameters are followed by each system's parallax in milliarcseconds (mas; column 6) and the reference for that value (column 7), the V magnitude and reference (columns 8 and 9), and the $V-K$ color (column 10), where K is from 2MASS (Cutri et al. 2003). Given next are the subsets to which each target belongs (columns 11–13, described in detail below) and flags (column 14) for whether the system has been resolved (Y) or not resolved (N) thus far at SOAR (N/A indicates not yet observed), with the flag "T2" marking systems with results presented in Table 2. Finally, a reference for the orbit of a system is given (column 15), if it exists, with flag "T4" in this column marking systems with orbits presented in this work (Section 4.3).

The target list of 338 systems is drawn from three sources: astrometric multiples identified through long-term RECONS data (Jao et al. 2005; Henry et al. 2018), known multiples from the literature with potential $P_{\rm orb}<30$ yr, and suspected

[7] A few systems do not meet the 25 pc distance cutoff using updated parallaxes from Gaia EDR3 (Gaia Collaboration et al. 2021) which was released after this SOAR program began.

Table 1
Target List for the SOAR Speckle Program for 25 pc M Dwarfs

R.A. J2000.0 (1)	Decl. J2000.0 (2)	WDS (3)[a]	Discov. Code (4)	Name (5)	π (mas) (6)	π References (7)[b]	V (mag) (8)	V References (9)	$V-K$ (mag) (10)[c]	0.9m PB (11)[d]	Lit. mult. (12)[d]	DR2 sus. (13)[d]	SOAR References (14)[e]	Orbit References (15)[f]
00 06 39.24	−07 05 35.9	00067−0706	JNN 11	2MA0006-0705AB	46.960 ± 0.403	EDR3	14.72	APdr9	5.76		✓	✓	N, T2	
00 08 53.92	+20 50 25.6	00089+2050	BEU 1	G131-026AB	55.256 ± 0.761	DR2	13.52	Rie14	5.51	✓	✓	✓	Y	T3
00 09 45.04	−42 01 39.3	00098−4202		LEHPM1-0255AB	60.889 ± 0.350	EDR3	13.62	Win15	5.40			✓	Y, T2	
00 13 46.60	−04 57 37.2	00138−0458		LHS1042	42.627 ± 0.219	EDR3	17.98	estim	7.50			✓	N, T2	
00 15 27.99	−16 08 01.8	00155−1608	HEI 299	GJ1005AB	169.522 ± 0.969	Vri20	11.48	Win15	5.09	✓	✓	✓	Y	Ben16
00 15 58.07	−16 36 57.6	00160−1637	BWL 2	2MA0015-1636AB	56.096 ± 0.093	EDR3	13.20	Win19	5.29		✓	✓	Y	T3
00 16 01.97	−48 15 39.1	00160−4816	TOK 808	L290-072AB	40.672 ± 0.525	EDR3	11.55	Koe10	4.44		✓	✓	Y	
00 16 14.63	+19 51 37.5	00162+1952		GJ1006AC	65.108 ± 0.041	EDR3	12.26	Wei96	5.17		✓	✓	Y, T2	
00 21 37.26	−46 05 33.4	00216−4606		L290-028	51.569 ± 0.045	EDR3	12.24	Koe10	4.79			✓	N, T2	
00 24 44.19	−27 08 24.2	00247−2653	LEI 1AB	GJ2005AB	129.317 ± 0.126	EDR3	15.28	Win15	7.04	✓	✓	✓	Y	Koe12

Notes.
[a] Column 3—For all systems not already noted in the WDS catalog (Mason et al. 2001), the WDS code given is the anticipated code for the future entry should these systems be resolved.
[b] Column 7—The parallax reference is "EDR3" for Gaia EDR3 (Gaia Collaboration et al. 2021) "DR2" for DR2 (Gaia Collaboration et al. 2018), or other references as listed in the Table notes.
[c] Column 10—Reference for all K magnitudes in $V-K$ color is (Cutri et al. 2003).
[d] Columns 11–13—These are classification flags indicating the subsets to which each system belongs: 0.9 m PB = system with perturbation in RECONS astrometry residuals (Section 2.1), Lit. mult. = known binary from the literature (Section 2.2), DR2 sus. = system with evidence of multiplicity in Gaia DR2 results (Section 2.3). Check marks in parentheses (✓) in column 12 indicate unpublished results from coauthor Winters (to be published speckle survey results).
[e] Column 14—This column indicates SOAR resolutions and nonresolutions as presented in previous papers in the yearly SOAR series (e.g., Tokovinin et al. 2019, 2020, 2021), except those noted with the "T2" flag, which are given in Table 2.
[f] Column 15—This column gives the reference for the existing orbit in the literature from the Sixth Catalog of Orbits of Visual Binary Stars (Hartkopf et al. 2001), with flag "T4" noting orbits newly presented in this work in Table 4 and Figure 2.
References. * = This work, APdr9 = Henden et al. (2016), And07 = Andrade (2007), Ben16 = Benedict et al. (2016), Bur15b = Burgasser et al. (2015), Cal17 = Calissendorff et al. (2017), Dah88 = Dahn et al. (1988), Dit14 = Dittmann et al. (2014), Doc19 = Docobo et al. (2019), Dup10b = Dupuy et al. (2010), Dup16 = Dupuy et al. (2016), For99 = Forveille et al. (1999), EDR3 = Gaia EDR3 (Gaia Collaboration et al. 2021), DR2 = Gaia DR2 (Gaia Collaboration et al. 2018), Hei94 = Heintz (1994), Hen18 = Henry et al. (2018), HIP07 = van Leeuwen (2007), Izm19 = Izmailov (2019), Jao14 = Jao et al. (2014), Ker16 = Kervella et al. (2016), Koe10 = Koen et al. (2010), Koe12 = Köhler et al. (2012), Kon10 = Konopacky et al. (2010), Lur14 = Lurie et al. (2014), Man19 = Mann et al. (2019), Mas18 = Mason et al. (2018), Rie10 = Riedel et al. (2010), Rie14 = Riedel et al. (2014), Rie18 = Riedel et al. (2018), Seg00 = Ségransan et al. (2000), Sca19 = Scardia et al. (2019), Sod99 = Söderhjelm (1999), Tok15c = Tokovinin et al. (2015), Tok17b = Tokovinin (2017), Tok18a = Tokovinin (2018a), Tok18c = Tokovinin (2018c), Tok19c = Tokovinin et al. (2019), Tok19b = Tokovinin (2019), Tok20a = Tokovinin (2020), Tok20b = Tokovinin et al. (2020), Vri20 = Vrijmoet et al. (2020), Wei96 = Weis (1996), Win15 = Winters et al. (2015), Win17 = Winters et al. (2017), Win19 = Winters et al. (2019), Zir03 = Zirm (2003).

(This table is available in its entirety in machine-readable form.)

Table 2
Results of Observations Through 2020 in the SOAR Speckle Program for 25 pc M Dwarfs

WDS (1)[a]	First res. (2)[b]	Date Obs. (yr) (3)	Resol. (Y/N) (4)	ρ ($''$) (5)[c]	θ (deg) (6)[c]	Δm (mag) (7)[c]	ρ_{min} ($''$) (8)[d]	Δm (0.″15) (mag) (9)[d]	Δm (1.″0) (mag) (10)[d]	Obs. Flags (11)[e]
00067−0706	Jan14	2019.8568	N				0.0768	2.3	2.9	
		2020.8342	N				0.0594	2.3	2.8	
00098−4202	*	2019.6133	Y	0.0522	159.0	0.8				
		2019.8567	N				0.0525	2.5	3.9	
		2020.8341	Y	0.0959	115.7	1.0				
		2020.9270	Y	0.1089	117.4	0.9				q
00138−0458	none	2019.8568	N				0.1145	1.6	2.5	:
		2020.8342	N				0.1260	1.6	1.6	:
00162+1952	*	2019.5397	N				0.0636	2.3	3.9	
		2019.8564	N				0.0543	2.7	4.1	

Notes. All magnitude differences are in the *I* band, except where the *y* band is noted in column 11.
[a] Column 1—For resolved systems not already noted in the WDS catalog (Mason et al. 2001), the WDS code given is the anticipated code for the future entry.
[b] Column 2—This column gives a single or double asterisk (* or **) for each new resolution, depending on previous status of the target's multiplicity. A single asterisk (*) indicates a new resolution of a system already known in the literature to be a multiple, but which has never previously been resolved. A double asterisk (**) marks a new resolution of a system that was previously a multiple candidate at best, with its multiplicity not established in the literature; these are new multiples. Systems previously resolved by others have their first resolution reference listed. Systems not resolved here and never resolved previously are noted with "none" in this column.
[c] Columns 5–7—For observations that resolved a companion, these columns give the separation (ρ), position angle (θ), and magnitude difference (Δm) between components.
[d] Columns 8–10—For observations with no detected companion, these columns provide limits: the minimum separation distinguishable (ρ_{min}) for pairs with $\Delta m < 1$ mag, the magnitude difference limit at 0.″15 from the primary source, and the magnitude difference limit at 1.″0 from the source.
[e] Column 11—This column contains flags related to each observation: q = quadrant has been determined, p = Δm determined photometrically from average image, : = noisy data, *y* = magnitude difference in *y* band (all others in *I* band).
References. Jan14 = Janson et al. (2014), Jao14 = Jao et al. (2014), Jod13 = Jódar et al. (2013), Kar20 = Karmakar et al. (2020), Mar00 = Martín et al. (2000), War15 = Ward-Duong et al. (2015).
(This table is available in its entirety in machine-readable form.)

multiples chosen based on their Gaia DR2 results (criteria described in Vrijmoet et al. 2020). As illustrated in Figure 1, these subsets overlap each other—for example, some systems from RECONS astrometry are already known multiples in the literature—and in the target list in Table 1 we have indicated each target's subset membership using columns 11–13. The selection and goals for each of these groups is described next.

2.1. 123 Targets from the RECONS Astrometry Program

The RECONS program (Jao et al. 2005; Henry et al. 2018) began taking astrometry data in 1999, targeting red, brown, and white dwarfs within 25 pc. Through 4–6 observing runs per year at the SMARTS 0.9 m at CTIO, this program has been mapping the motions of several hundred nearby stars for a median duration of 10 yr. This enables the detection of binaries with orbital periods many decades in length, with orbital characterization possible for P_{orb} up to ∼30 yr in the longest-observed cases. Fully observed orbits are fit using the Markov Chain Monte Carlo method introduced in Dieterich et al. (2018), which simultaneously fits the proper motion, parallax, and orbital motion of the system's photocenter; nine examples with P_{orb} from 2 to 17 yr using RECONS data from the 0.9 m are given in Vrijmoet et al. (2020).

RECONS astrometry qualified the selection of 123 targets for the SOAR observing list, with 37 of these targets not qualifying for either of the other two subsets. Systems were considered high priority if their residuals to the parallax and proper motion fit exhibited perturbations (PBs) that were characteristic of orbital motion due to bound companions. These residuals are considered significant perturbations if their maximum amplitude is at least three times the size of the average error per epoch for that system (with these errors typically 3–5 mas). In many cases these residuals clearly traced out orbital motion by the system's photocenter, with a smooth rise and fall in R.A. and/or decl. axes, depending on orbital coverage, observing cadence, and the particular orbit shape. Orbital period can be estimated by eye in these cases, or constrained by a preliminary fit to an astrometric orbit model.

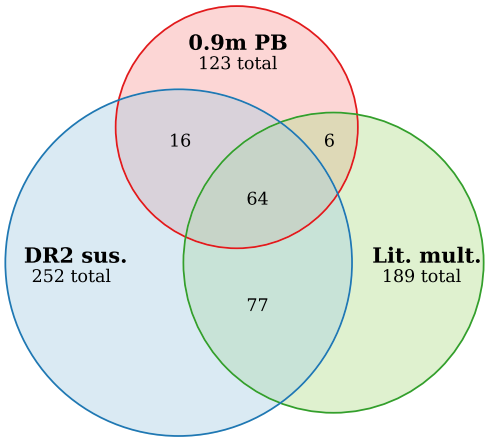

Figure 1. Venn diagram illustrating the three subsets of the SOAR sample of nearby M dwarfs. The area of each circle is proportional to the number of targets in that subset, but the overlapping regions are not to scale. Each circle is labeled with a reference to the subset's source: "0.9 m PB" for targets showing perturbations (PBs) in the RECONS astrometry program at the CTIO 0.9 m, "Lit. mult." for known literature multiples, and "DR2 sus." for systems suspected to be multiples based on their Gaia DR2 results. The number of targets is given under each subset name, and the numbers in the overlapping sections indicate the number of targets common to multiple subsets.

Targets were selected for our SOAR speckle campaign if these residuals thus indicated an orbit with likely $P_{\rm orb} \lesssim 30$ yr. In other select cases the residuals were clearly perturbed but the motion was more difficult to interpret, which may occur when an orbit shorter than ~3 yr is observed with the relatively sparse cadence of the RECONS observations or the PB is weak because two components have similar fluxes and the photocenter consequently moves very little.

The goals for the "0.9 m PB" subset (column 11 in Table 1) are thus twofold:

1. For systems with orbits that can be fully characterized in the RECONS astrometry, resolving the components will allow us to determine their individual dynamical masses (following the methods outlined in van de Kamp 1967).
2. For targets with PBs that are ambiguous rather than clearly due to orbital motion, resolving a second star will confirm that companion and constrain its orbit, aiding interpretation of the RECONS astrometric residuals and ongoing observing priorities for the 0.9 m program.

In both cases, nondetections will place constraints on the natures of the potential companions and their orbits, and in some cases (notably, in the unclear ones) nondetections will allow us to rule out a companion as the source of the astrometric residuals.

2.2. 189 Targets from Known Multiples in the Literature

To enrich the sample, and because astrometry is less sensitive to some types of binaries (e.g., equal-luminosity components), the SOAR target list was augmented with known M-dwarf multiples from the literature. These known multiples constitute 189 targets, with 42 not belonging to either of the other subsets. Our observations are intended to capture orbital motion, so these targets were limited to pairs that had previously been resolved at separations $\lesssim 2\farcs0$ or likely orbital periods less than 30 yr. Not all of these pairs have been resolved in the literature; about a third are known multiples based on only spectroscopic or astrometric results. These systems were primarily selected by cross-matching the Sixth Catalog of Orbits of Visual Binary Stars (Hartkopf et al. 2001) against coordinates of M dwarfs from Gaia DR2 and the RECONS astrometry target list. These were augmented by some M-dwarf multiples from the Washington Double Star Catalog (WDS; Mason et al. 2001) and private communications from collaborators.

The intention of the observations for this "Literature multiples" subset (column 12 of Table 1) is to add new measurements to the existing data sets for each system, with the following goals:

1. Enable fitting of each system's relative orbit by extending the time baseline of observations.
2. Improve upon any existing orbit fits, in particular by refining the precision of the orbital elements.

2.3. 252 Targets Selected from Gaia DR2

Gaia DR2 (Gaia Collaboration et al. 2016, 2018) released proper motions and parallaxes for ~1.7 billion sources based on an astrometric model that includes only those two sources of motion, with orbital motion fits not planned until future data releases. Systems exhibiting orbital motion from a bound companion should thus exhibit evidence of poor astrometric fits. Vrijmoet et al. (2020) showed that nearby M dwarfs with unresolved companions can be selected based on several DR2 fit parameters, akin to the astrometric residuals in RECONS data (Section 2.1).

Gaia DR2 results were used to identify 252 total M dwarfs for the SOAR observing list, with DR2 being the only source of potential multiplicity for 95 targets. This evidence is based on the analysis of Vrijmoet et al. (2020), and most of these "DR2 suspects" met at least some of the final criteria presented there. Those specific DR2 criteria identified in Vrijmoet et al. (2020) were:

1. missing parallax or missing catalog entry,
2. `parallax_err` $\geqslant 0.32$ mas for $G \lesssim 18$ ($\geqslant 0.40$ mas otherwise),
3. `astrometric_gof_al` $\geqslant 56.0$,
4. `astrometric_excess_noise` $\geqslant 108.0$, and
5. `ruwe` $\geqslant 2.0$.

That work found that at least three out of four systems meeting at least one of these thresholds were multiples unresolved in DR2. While selecting targets for this subset of SOAR observations, we anticipated that the values of these criteria may eventually be lowered if many stars that were presumed single are later revealed to be binary.

The goals for this group of "DR2 suspects"(column 13 of Table 1) are:

1. Map orbits of new multiples with periods that will be at least 50% complete by the end of this 3 yr observing campaign (i.e., with $P_{\rm orb} \lesssim 6$ yr). The DR2 selection criteria should be more sensitive to these particular systems because of its relatively short observing baseline of 22 months.
2. Confirm the validity of the Vrijmoet et al. (2020) criteria for selecting binaries from Gaia DR2 via the resolution of companions, and revise the criteria if necessary.

3. Observations and Data Reduction with HRCam+SAM

The observations presented here were made over 2018–2020, with most completed between 2019 July and 2020 December, representing the first half of our planned 3 yr program. Many systems in our sample were already observed at SOAR prior to this project as part of earlier initiatives to investigate M dwarfs in the Southern Hemisphere. Their results do not appear in Table 2 because those results were presented in previous SOAR papers (Tokovinin et al. 2021, 2020); instead, they have a "Y" or "N" in column 13 of Table 1 with no additional flags.

Time awarded for the speckle observing programs of coauthors Tokovinin and Vrijmoet was combined in order to increase the opportunities for timely observations of fast-orbiting systems. In preparation for each observing run, previous SOAR observations and RECONS astrometry were considered, and systems that had exhibited rapid orbital motion were prioritized for the upcoming run. This procedure improved the likelihood that defining features of the orbit shapes would not be missed.

All of the observations used HRCam, the high-resolution camera mounted on the SOAR Adaptive Module (SAM; Tokovinin et al. 2016), in the seeing-limited mode (no laser guide star was used). Frames were taken almost exclusively in

the Kron–Cousins I filter, usually in 2–3 sets (data cubes) of 400 frames per target, with integrations typically 24 ms per frame. These sets were each later processed independently to verify results. Most observations use the HRCam narrow 3″ field of 200×200 pixels, whereas pairs known to have separations of 1.″4 or more were observed with the 400×400 field. The resolution limit in I is usually 40–45 mas depending on target brightness and sky conditions, but can be as close as 35 mas in some cases (see Figure 1 of Tokovinin et al. 2020). Targets that are unresolved in the first two attempts are usually observed a third time, then retired from the program if still unresolved.

The data are processed and reduced for this program using the standard procedures described in Tokovinin et al. (2010) and Tokovinin (2018b), and representative images of the reduced data products are shown in Tokovinin (2018b). In brief, for each target the power spectrum and autocorrelation function are calculated, and companions are noted via power spectrum fringes or secondary peaks in the autocorrelation function. Fitting an empirical model to the power spectrum yields the parameters of each detected pair: the separation between components (ρ), the position angle of the secondary with respect to primary star (θ) (north = 0° through east = 90°), and the difference in magnitude between components (Δm). Important details about these results are:

1. The position angle determined through this procedure is only ascertainable modulo 180°, leaving some ambiguity in the secondary's true position on the sky. This ambiguity has been eliminated whenever possible by applying a shift-and-add procedure to each target's data (Tokovinin 2018b); this process reveals the true quadrant for companions that are not too faint but still have some magnitude difference with their primary star ($\Delta m \gtrsim 0$ mag). These results are noted with the "q" flag in Table 2, indicating that the quadrant has been determined.
2. For some observations of wider pairs a separate procedure is used to determine the magnitude difference using the average image for a target (described in detail in Tokovinin et al. 2010). This method produces more reliable photometry for these cases where the stars' separations are greater than image resolution, reducing bias from speckle anisoplanatism. Observations with Δm determined with this method are marked by a "p" in Table 2, indicating that this photometric method has been used.
3. For observations in which no companion was detected, a contrast curve is computed to report the detection (magnitude) limits as a function of the distance from primary star on the sky (for example, see Figure 5 of Tokovinin 2018b). The parameters of this curve are reported in the results in Table 2 as the minimum separation resolvable for pairs with $\Delta m < 1$ mag, as determined from the maximum spatial frequency of the power spectrum, and the maximum detectable magnitude difference at separations of 0.″15 and 1.″0 (the dynamic range).

4. Results

Through the end of 2020 and including previously published results, 333 targets on this program have been observed at least once at SOAR via 830 total observations. Of these targets, 211 (63% of the total sample) had a companion detected at least once, representing 204 total systems.[8] In this first half of our 3 yr program, most companions were observed numerous times to confirm that the detected object was a true companion and not a background source; the remainder have follow-up observations planned. For each true multiple, these initial observations will then contribute to that system's orbit mapping.

The results are detailed in Table 2 for both newly resolved and unresolved systems. Targets with previous resolutions appear instead in the yearly SOAR publication series (e.g., Tokovinin et al. 2020, 2021). Table 2 gives the WDS coordinate name or anticipated WDS name in column 1. In column 2 is either the reference for the first resolution of that system, a single asterisk (*) for the first resolution of a known multiple, two asterisks (**) for the first resolution of a system that was previously, at best, only a candidate multiple (see Section 4.1 for details), or "none" if the system was not resolved. Each observation of a target is then distinguished by its date (column 3) and Y/N flag for whether or not the companion was detected at that epoch (column 4). Observations in which the companion was resolved include the separation, position angle, and magnitude difference between components (columns 5–7). Observations with no detected companion list the minimum resolution detectable and Δm limits at 0.″15 and 1.″0 from the primary star, respectively (columns 8–10). Finally, observation flags (column 11) note several of the cases described in Section 3, such as when the quadrant of the position angle is unambiguously determined (q), when the magnitude difference was determined photometrically from the average image (p), when the observations resulted in noisy data (:), generally leading to less robust limits, or y for the one observation done through a y filter rather than the I filter.

Uncertainties on the individual measurements are not listed here, as these would require a more detailed analysis than feasible for this paper. The full measurement errors consist of internal errors, which could be determined by comparing each observation's data cubes, and external errors, which can be estimated from HRCam measurements of well-characterized binaries ("calibrators"), Gaia-resolved sources (Tokovinin et al. 2019), and residuals of each system's orbital fit. The typical deviation of the calibrators from their orbit models is 1–3 mas in separation and 0.°2 in position angle, and in a similar procedure with SOAR speckle data, Mann et al. (2019) found errors of 3.8 mas and 0.°94 are appropriate additions to the internal errors (typically $\leqslant$2 mas). For this reason we have assigned errors of 5 mas to all SOAR HRCam measurements when fitting orbits, and postponed the full derivation of external errors until this 3 yr observing program is complete. See Section 4.3 for additional details of the orbit fitting routine.

4.1. Detections

Table 3 summarizes the detection rates for each group within the full sample (Section 2). For each named subset (column 1), it provides the number of targets observed (column 2), the number resolved (column 3), the percentage of observed targets

[8] In seven cases, a higher-order multiple with two components separated by a few arcseconds represents two targets for this speckle survey, and as such is represented by two lines in Table 1 (and counts as two targets throughout this paper).

Table 3
Summary of SOAR Speckle Results for Each of the three Sample Subsets, as Well as the Targets Meeting the Formal Multiplicity Criteria in DR2 (Vrijmoet et al. 2020) and the Full Sample

Subset Name (1)	Targets Observed (2)	Pairs Resolved (3)	Percent Resolved (4)	Targets Not Observed (5)
0.9 m PB	120	59	49%	3
Literature multiples	188	140	74%	1
DR2 suspects	249	188	76%	3
2+ DR2 criteria	217	176	81%	2
Full sample[a]	333	211	63%	5

Note.
[a] Numbers are not the sums of the four categories above because of overlaps in samples, as shown in the Venn diagram of Figure 1.

that were resolved (column 4), and the number of targets not yet observed by the end of 2020 (column 5).

Of the 211 companions resolved in our sample, 97 had no previously published resolutions, making these results their first published positional measurements. These newly resolved systems are marked with asterisks in column 2 of Table 2, broken into two categories. A single asterisk (*) denotes the 34 systems that were already reported to be multiples based on other published data, e.g., astrometry or spectroscopy. A double asterisk (**) denotes new resolutions for 63 systems with no previously reported multiplicity in the literature—these were included in the target list due to anomalies in their RECONS or Gaia DR2 astrometry. These are newly discovered multiples in addition to being new resolutions.

Additionally, 114 companions noted here as resolved at SOAR already had resolutions in the literature; nearly all of these systems are listed as "Y" in Table 1 but without the "T2" flag, as they are presented in Tokovinin et al. (2020, 2021), and previous publications in that yearly series. Column 2 of Table 2 gives the reference for the first resolution of that system. For all systems with data already in the literature, the new observations presented here and in the other SOAR results papers will ultimately be combined with previous results to improve orbital coverage. We have already employed this strategy for the orbits we are presenting here (Section 4.3).

Data from the RECONS astrometry program at the SMARTS 0.9 m already reveals perturbations in 59 of the 211 resolved pairs. That astrometry provides maps of the photocentric orbits, hence the resolutions of companions in these cases will enable us to solve for the individual masses within each pair as in, e.g., Dieterich et al. (2018). Each of these new masses will contribute to the currently modest number of dynamically determined individual M-dwarf masses known to date (Benedict et al. 2016).

Finally, there are 249 targets observed (and 3 targets not observed) that showed some evidence of poor astrometric fits in Gaia DR2 and were included based on preliminary results of the Vrijmoet et al. (2020) analysis. Our SOAR observations reveal that 188 (76%) of these M dwarfs host a companion. This result highlights the utility of that method of selecting likely multiples using Gaia's astrometric fit parameters, especially for these nearby, low-mass systems. See Section 5.4 for further discussion of this result, details about the DR2 criteria outlined in Table 2, and the implications.

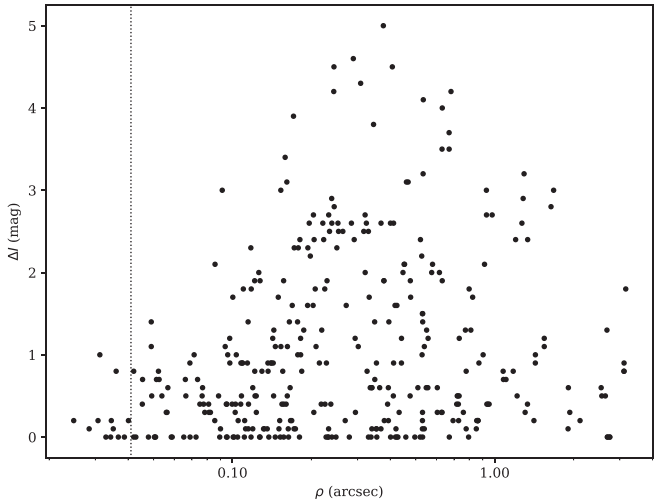

Figure 2. Separation ρ in arcsec and magnitude difference in I band for each observation that resolved a companion, excluding those for which the data were exceptionally noisy (":" flag in Table 2). The 41 mas formal diffraction limit of SOAR is indicated with the vertical dotted line. This sample is intentionally focused on the closer pairs ($\lesssim 1\farcs0$) that are more likely to show orbital motion over our 3 yr campaign.

Figure 2 shows the separations (ρ) and magnitude differences in I band (ΔI) for each observation that detected a companion. This distribution of exclusively M dwarfs is similar to that of the wider sample observed yearly by SOAR (shown in Figure 1 of Tokovinin et al. 2020). The most notable difference is our distribution shows a paucity of systems with $\Delta I > 1.5$ mag and $\rho < 0\farcs1$. This discrepancy could reflect the higher fraction of very faint companions in our sample compared to the other samples observed yearly at SOAR. The mass–luminosity relation is known to experience a severe drop at optical wavelengths at low M-dwarf masses (Benedict et al. 2016). Therefore, it is not surprising that companions only slightly less massive than their primaries may have large ΔI values compared to their primaries and remain undetected at SOAR.

4.2. Nondetections

The 122 targets observed with no companions detected at SOAR still impart important information via the detection limits given in columns 8–10 of Table 2. Because these observations were conducted in the I filter, in many cases these nondetections restrict potential companions to the regimes of cool white dwarfs, very-low-mass stars, or brown dwarfs. Examples include LHS 1582 AB (03434−0934), SCR 0723-8015 AB (07240−8015), and LP 848-50 AB (10427−2416), all of which exhibit clear orbital motion in their long-term astrometry (Winters et al. 2017; Vrijmoet et al. 2020). Other true multiples unresolved here may have orbits too tight to resolve, or have components positioned unluckily too close to each other on the sky at the epoch of observation. In each of these cases, the nondetection information given here provides constraints on orbits and companion masses that can be used in concert with other efforts to reveal information about any unseen and/or undetected companions.

4.3. Orbits

Here we present five orbits fit using the SOAR observations, often combined with additional data available in the literature;

all but LHS 501 AC are the first orbits for the systems. These five orbits represent the highest-quality fits possible with the data from this program thus far, and fortuitously are also representative of the range of size and timescales accessible to this program. The orbital periods range from 0.67 to 29 yr, and each has at least four observations taken during the first 1.5 yr of this observing program. The full orbital parameters are given in Table 4 and illustrations of the fits are shown in Figure 3. Each data set was fit with the ORBIT code (Tokovinin 2016), which uses the Leavenberg–Marquardt least-squares method to identify the model orbit that best fits the weighted observations. The weights are inversely proportional to the errors on each point, which for these observations have been set to the typical external HRCam errors of 5 mas, and for literature observations are set to the published errors. The resulting fits have errors ranging from 0.3%–7.2% in orbital period and 1.3%–6.7% in semimajor axis. These errors on the orbital parameters are determined by the fitting algorithm.

Each system with an orbit fit is discussed briefly below. In each case we also provide estimates of the component masses using our work toward a mass–luminosity relation in I band (Vrijmoet et al. 2021). These estimates should be considered preliminary and are only intended as general guides of the mass regimes for these M dwarfs.

1. G 131-26 AB (00089+2050, BEU 1) is a known flare star with a stellar companion first detected by Beuzit et al. (2004) in 2001, then resolved again in 2012 by Janson et al. (2014) and in 2014 by Horch et al. (2015). We have resolved it four additional times in 2019–2020 and fit all of these data together to determine an orbital period of 5.918 ± 0.017 yr. Combining this orbit with the Gaia EDR3 parallax indicates a total system mass of $0.51 \pm 0.05\ M_{\odot}$. The individual components' M_I values are consistent with 0.3 $M_{\odot}$ and 0.2 $M_{\odot}$, a good match to the system total mass.
2. 2MA 0015-1636 AB (00160−1637, BWL 2) was resolved by Bowler et al. (2015) in 2011, who suggested an orbital period of 4.5 yr based on their observed separation. With our additional five points we find an orbital period of 4.187 ± 0.039 yr, yielding a total mass of $0.41 \pm 0.08\ M_{\odot}$ using the EDR3 parallax. The individual components' absolute magnitudes imply masses of 0.25–0.3 $M_{\odot}$ for each component. These values are somewhat higher than indicated by the total dynamical mass, pointing to some inaccuracy in the orbit or the parallax. This is validated by the Gaia reduced unit weight error (RUWE) value of 4.1, indicating the parallax is not well fit. The mass discrepancy would be eliminated by a 7% smaller parallax, or by increasing the orbit's semimajor axis by 7% or decreasing its period by 10%. Continued observations at SOAR will allow us to refine the orbit, and future Gaia data releases will likewise improve the system's parallax.
3. LP 993-115 BC (02452−4344, BRG 15Aa,Ab), also known as LP 993-116 AB, is a common proper motion companion to LP 993-115 A (44″; Bidelman 1985). The C component was first identified by Bergfors et al. (2010) with lucky imaging and resolutions also reported in Janson et al. (2012, 2014). We add four new resolutions to map the other side of the orbit, and derive a period of 28.466 ± 2.056 yr. Using the EDR3 parallax, this suggests a total mass of $0.42 \pm 0.23\ M_{\odot}$ for BC, although this value is poorly constrained. Individual absolute magnitudes for the B and C components are consistent with component masses of 0.2–0.25 $M_{\odot}$ each. This is the first orbit published for this subsystem of this higher-order multiple.
4. SCR 0533-4257 AB (05335−4257, SYU 7Aa,Ab) was first resolved by Shan et al. (2017) in 2014, and to this we have added six points in 2019–2020. With an orbital period 0.672 ± 0.003 yr, the orbit and EDR3 parallax indicate a total mass of $0.40 \pm 0.07\ M_{\odot}$. This is consistent with the possible period of 9 months noted in the unresolved RECONS astrometry by Riedel et al. (2018). The individual absolute magnitudes of each component are consistent with 0.25 $M_{\odot}$ and 0.15 $M_{\odot}$, together an excellent match to the total dynamical mass.
5. LHS 501 AC (20556−1402) is a now-resolved primary with a wide companion known as LHS 500, separated by 107″ (Jao et al. 2003). The AC pair had not been resolved prior to this work, but was noted to be an astrometric multiple by Jao et al. (2011) based on the RECONS astrometry data. Baroch et al. (2018) noted it to be SB2 and presented a spectroscopic orbit fit. Our new orbit was fit to their spectroscopic data simultaneously with our four new visual resolutions using the same ORBIT code as for the other four orbits in this work. The resulting orbital period of 1.855 ± 0.014 yr is shorter in length but ten times more precise than the Baroch et al. (2018) period (2.22 ± 0.16 yr). Our eccentricity is also significantly different, at 0.242 ± 0.008 versus their 0.402 ± 0.059. Additional observations underway will significantly improve future orbit fits for this system, as the radial velocity model still shows some minor discrepancies with the data (lower rightmost panel of Figure 3). With our result and the EDR3 parallax we derive a total mass of $0.37 \pm 0.02\ M_{\odot}$. The individual absolute magnitudes correspond to stars with masses of 0.25 $M_{\odot}$ and 0.2 $M_{\odot}$, which is roughly consistent to the total dynamical mass, although future refinement will be necessary for this orbit.

5. Discussion

As outlined in Section 1, our goal is to catalog at least 120 orbits with $P_{\rm orb} \leqslant 30$ yr with reliably determined orbital periods and eccentricities through the combination of this 3 yr speckle campaign, the long-term RECONS astrometry program at the SMARTS 0.9 m, and orbits in the literature. A set representing orbits out to (at least) 30 yr periods will be necessary to draw significant conclusions about the formation and evolution of these systems. Selecting 120 orbits evenly distributed in orbital period will ensure that there are ∼20 orbits in each 5 yr bin of $P_{\rm orb}$ in the final $P_{\rm orb}$ versus e plot. More fundamentally, the goal of 120 orbits is a compromise between the need to characterize the $P_{\rm orb}$ versus e relation with maximum detail and a realistic expectation based on our prior experience and availability of resources.

The abundance of detected companions and promising initial orbit fits resulting from this first phase of our SOAR effort provide several advances toward the overall project regarding orbit distributions of M-dwarf multiples. For all systems in Table 2, both the resolutions and nonresolutions reported here provide valuable constraints on the orbits of their companions

Table 4
Elements of the Best-fit Relative Orbits Shown in Figure 3

Name	WDS	Discov Code	P (yr)	a (mas)	e	i (deg)	Ω (deg)	ω (deg)	T_0 (yr)	Additional Data Used
(1)	(2)	(3)	(6)	(7)	(8)	(9)	(10)	(11)	(12)	(13)
G 131-026 AB	00089+2050	BEU 1	5.918 ± 0.017	144.0 ± 4.6	0.106 ± 0.023	145.67 ± 3.29	83.61 ± 6.59	240.38 ± 17.17	2018.921 ± 0.173	Beu04, Jan14, Hor15
2MA 0015-1636 AB	00160−1637	BWL 2	4.187 ± 0.039	108.0 ± 7.2	0.433 ± 0.090	63.63 ± 2.11	111.81 ± 5.15	98.03 ± 4.82	2021.145 ± 0.057	Bow15
LP 993-115 BC	02452−4344	BRG 15Aa,Ab	28.466 ± 2.056	630.3 ± 37.5	0.240 ± 0.029	117.13 ± 1.98	158.70 ± 1.01	305.03 ± 8.74	2009.714 ± 0.434	Ber10, Jan12, Jan14
SCR 0533-4257 AB	05335−4257	SYU 7	0.672 ± 0.003	54.4 ± 3.3	0.490 ± 0.066	150.73 ± 9.59	109.41 ± 29.17	44.38 ± 9.59	2017.155 ± 0.013	Sha17
LHS 501 AC	20556−1402	... ...	1.855 ± 0.014	91.6 ± 1.2	0.242 ± 0.008	142.67 ± 2.11	236.06 ± 2.46	232.05 ± 1.88	2017.135 ± 0.009	Bar18[a]

Notes. These orbits have been fit to the relative positions of the systems' components using all resolutions (including literature and this SOAR program), as well as radial velocities if those data are available.
[a] RV data used in orbit fit.

References. Bar18 = Baroch et al. (2018), Ber10 = Bergfors et al. (2010), Beu04 = Beuzit et al. (2004), Bow15 = Bowler et al. (2015), Hor15 = Horch et al. (2015), Jan12 = Janson et al. (2012), Jan14 = Janson et al. (2014), Sha17 = Shan et al. (2017).

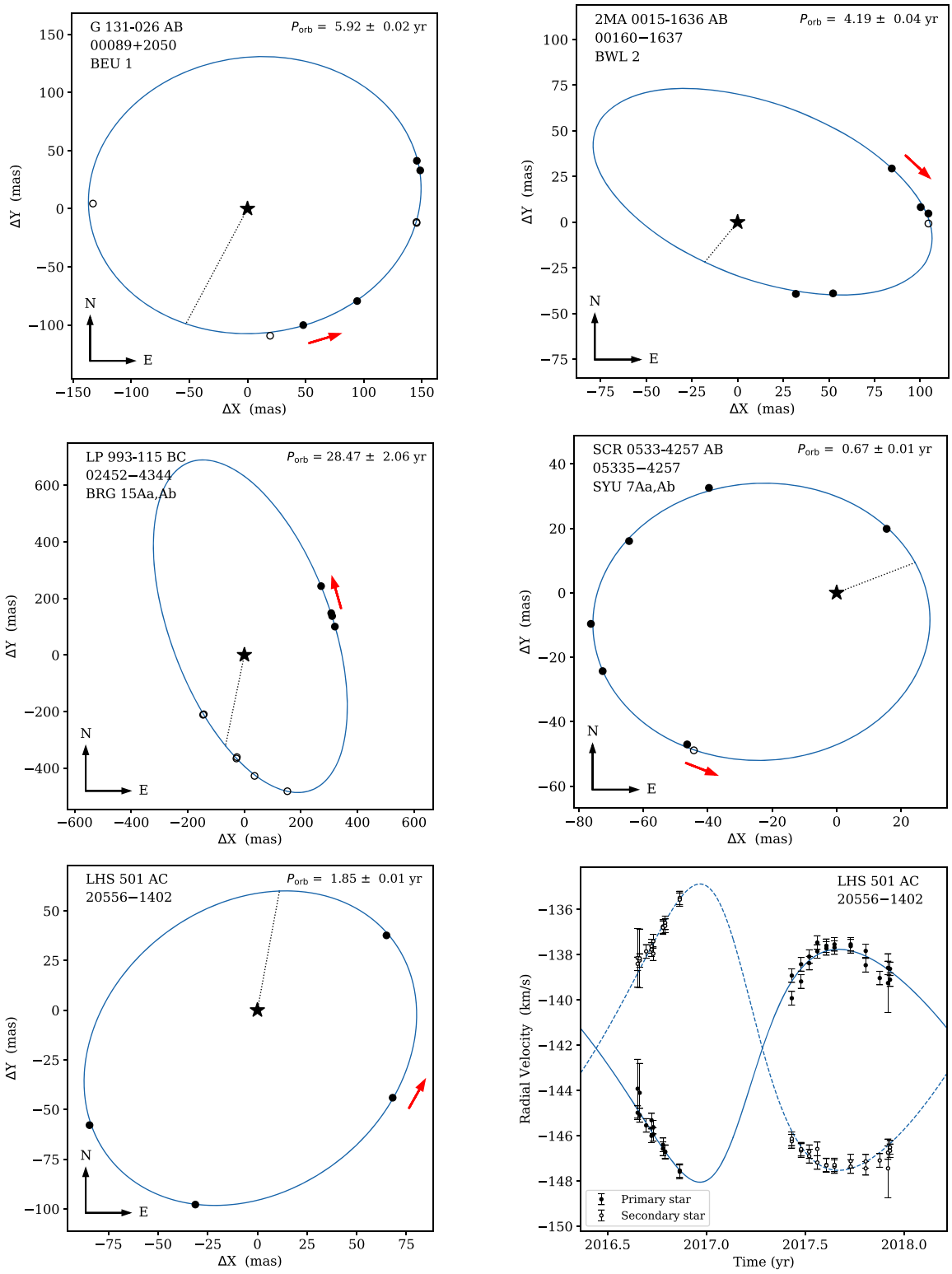

Figure 3. Five visual orbits for binaries resolved at SOAR, plus one spectroscopic orbit that was fit simultaneously with the corresponding visual orbit for LHS 501 AC. For the visual orbits, blue lines denote the fit, filled circles are SOAR observations, and open circles are observations added from the literature. Red arrows indicate the direction of motion of the secondary star around the primary, and the black star and dotted line denote the primary star and line of periastron, respectively. In the spectroscopic orbit (bottom right panel), the points and solid line are the observations and fit, respectively, for the primary component, and the open points and dashed line are the observations and fit for the secondary. Left to right, top to bottom: G 131-26 AB, 2MA 0015-1636 AB, LP 993-115 BC, SCR 0533-4257 AB, LHS 501 AC visual orbit, and LHS 501 AC radial velocity orbit (observations from Baroch et al. 2018). Sources for additional visual observations are specified in Table 4.

or the likelihood of each star's multiplicity. Notably, we have increased the total number of resolved M-dwarf multiples within 25 pc by 97, representing 194 targets for further study of M-dwarf multiples' properties. We have also secured

observations for 140 systems that had been previously resolved, providing not only new points for orbit determinations, but relative fluxes in the *I* band that can be used for a robust mass–luminosity relation at *I*. Finally, the five new orbits presented here can be added to the key $P_{\rm orb}$ versus *e* plot, and each new fit helps to identify reliable orbits as well as those for which more data are required to reach the orbital element precision needed to reveal clues about the star formation process.

5.1. Contributions to Nearby M-dwarf Orbits

As of 2021 July, ∼200 orbits in the Sixth Catalog of Orbits of Visual Binary Stars (Hartkopf et al. 2001) are those of M-dwarf systems within 25 pc. About one third of these have periods longer than 100 yr, and another third have periods 10–100 yr, with the remaining third shorter than 10 yr. Our SOAR program targeting orbits 0–6 yr is thus well poised to make a significant contribution to this catalog. All but one of the orbits presented here have $P_{\rm orb}$ in that range, demonstrating proof of concept for this plan.

Four of the five orbits presented here are new, while the fifth (LHS 501 AC) represents a substantial revision over the previously published result (Baroch et al. 2018). This set of orbit results is roughly representative of the expected yield of our program: for most orbits, we will combine existing data with our new data to produce fits for systems that previously had no published orbits. Several dozen more orbits will be updates to systems that already had solutions published; these will be a substantial fraction of the 73 targets in our sample that already have orbits in the literature listed with $P_{\rm orb} \leqslant 30$ yr.

Overall, we expect to fit at least ∼50 orbits using the full three years of observations planned for this program. This estimate is based on the number of systems already showing substantial motion over the first 1.5 yr of observations and includes improvement of published orbits as well as new orbits. These will substantially contribute to the 120-orbit goal to establish the M dwarf $P_{\rm orb}$ versus *e* distribution, supplementing the planned contributions from RECONS astrometry and the literature.

5.2. Implications for the RECONS Astrometry Subset (0.9 m PB)

Of the 120 systems observed from the 0.9 m PB list, 59 companions were detected using SOAR. Among these, 22 (37%) had not been resolved previously. The lower yield of this subsample compared to the other two is not too surprising because astrometry and speckle interferometry are each somewhat sensitive to different types of companions. Speckle searches are most sensitive to equal-luminosity components, but those systems exhibit no astrometric perturbation if both components are equal luminosity and have the same mass. In addition, many of the astrometric companions are likely very-low-mass stars or brown dwarfs that are beyond the magnitude difference limits of the speckle observations.

When no companion is detected with speckle, the magnitude limits reached at various separations constrain the nature of the astrometric companion and its orbit. Many cases in which these estimated mass limits were notable are described in detail in the Appendix. For each system, we have used the combined magnitude of the pair and the limiting magnitudes in the speckle results to estimate the components' fluxes, which we then combine with the size of the astrometric perturbation to estimate a limit for each companion mass (following van de Kamp 1967). Most of these systems have been described in previous work in *The Solar Neighborhood* series, often with plots showing their perturbed astrometric residuals, hence our descriptions here can be considered updates to those notes.

We used a similar procedure to estimate companion masses for the 0.9 m PB systems that SOAR did resolve. These masses (given in Appendix) are only rough estimates determined from the sizes of the photocentric displacements in the astrometric pertubations, rather than the fully characterized photocentric orbits. Future work will determine reliable photocentric orbits that can be combined with these SOAR resolutions to yield dynamical masses for the individual components.

5.3. Implications for the Known Literature Multiples Subset

Of the literature multiples, 140 out of 188 pairs observed were resolved at SOAR. These resolutions were the first ever for 34 of these systems, while 106 had been previously resolved by others. Of the 48 unresolved systems, nearly all were initially identified as multiples through *JHK* imaging or spectroscopic studies, hence their companions were likely too faint (e.g., brown dwarfs) or too closely bound (spectroscopic binaries) to resolve at SOAR in *I* band. The new resolutions are systems that often have complementary (nonimaging) data in the literature, and the previously resolved systems have imaging that precedes our SOAR results. Both cases will assist in our orbit fitting goals, as this extra information or lengthened time baseline both enable orbit fits to be made earlier than with our SOAR data alone. The five orbits presented here demonstrate that concept.

Our selected 30 yr orbital period limit is meant to capture as broad a picture of M-dwarf orbits as is feasible for a single observational program, in particular showcasing systems that fall between the widest binaries and those that are tightly bound because of tides. Inevitably, some of the systems we have resolved will prove to have orbits longer than our planned 30 yr limit, as many of these are wider pairs initially detected with less sensitive instruments. In these cases, the data from this campaign can be used to place constraints on those orbits, e.g., choosing appropriate cadences on these slow-moving systems to focus observations at future epochs when a companion moves quickly through its periastron passage. The ultimate contribution of multidecade orbits will thus come through observations collected over multiple projects, with updated orbits more precisely determined than currently possible. For now, our SOAR observations of these literature multiples provide a legacy data set that will contribute to future efforts long after our project is complete.

Long orbits can often be constrained by comparing their motions measured at two widely separated moments (e.g., Brandt et al. 2019; Currie et al. 2020; Bowler et al. 2021). These recent efforts use the Hipparcos-Gaia Catalog of Accelerations (HGCA; Brandt 2021), which has presented recalibrated proper motions of systems measured by the Hipparcos and Gaia missions, ∼30 yr apart. Another catalog based on the same principle has been compiled by Kervella et al. (2019). There are 60 systems on our program with an entry in the HCGA and many of these likely have accelerations evident in that catalog. By combining positional measurements with these proper motion changes, we could better constrain the orbits of these systems, especially those with very long periods.

We will consider the use of this approach in our future work on orbits.

5.4. Checking Criteria for Unresolved Multiples in Gaia DR2

A total of 249 of the 252 systems were observed from the DR2 suspects sample, selected at least partly based on their Gaia DR2 astrometric fits (91 stars were included based *only* on those fits). This subset was created because during the SOAR sample construction, the then-preliminary results of the Vrijmoet et al. (2020) analysis showed specific DR2 parameters to be reliable markers for unresolved multiplicity. The SOAR observations validate the defined markers, with companions detected for 188 stars (76% of that group). Many of these systems had no previously published resolved companions and are marked with ** in column 2 of Table 2.

The final analysis of Vrijmoet et al. (2020) ultimately listed five criteria that could be used to flag likely multiples in DR2 (given explicitly in Section 2.3): missing parallax or missing DR2 entry, and four threshold values of the DR2 astrometric fit parameters. That work involved constructing a sample of 542 RECONS parallax program targets that were cross-matched with Gaia DR2 results, and used those targets' multiplicity information to identify the DR2 astrometric fit parameters that best indicated the presence of unresolved companions. For each of these four identified parameters, threshold values were then determined, above which three out of four systems were unresolved multiples.

Of the 252 systems in our sample flagged in the preliminary stages of that DR2 analysis, 217 of the stars observed fulfill two or more of the final Vrijmoet et al. (2020) criteria. SOAR detected companions for 176 (81%) of these 217 targets, confirming that the majority of poor fits in DR2 were due to companions bright enough to detect with SOAR's HRCam +SAM. As Gaia's observing time baseline increases with future data releases, these fit flags will reveal multiples with longer orbital periods and fainter companions (smaller masses), as long as the Gaia data are fit with the single-star astrometric model. Clearly, Gaia data can be used to reveal many new potential stellar multiples before the final release of its binary star solutions.

For the 41 of 217 observed systems that fulfilled at least two of the criteria from Vrijmoet et al. (2020) but did not have a companion resolved, the presence of a companion cannot be fully ruled out. Indeed, roughly half of this subset have had their companions already confirmed through other means, such as spectroscopically or by showing unambiguous orbital motion in RECONS astrometry. Companions that are very faint or orbiting close to their primary stars will not be detectable with HRCam+SAM at SOAR; the largest magnitude difference observed here was $\Delta I = 5.0$ and the smallest separation seen was 24 mas. The DR2 suspects marked unresolved in Table 1 must still be regarded as likely multiples, and future observations are warranted to probe for very faint and very close-in companions.

To update the criteria for unresolved multiplicity of Gaia DR2 targets, we have added the new SOAR detections to the sample used in Vrijmoet et al. (2020). Although the sample used in that analysis was not volume complete beyond 13 pc, its proportion of multiples within any distance matched the observed multiplicity found by more comprehensive surveys (Winters et al. 2019). To preserve that feature and avoid overreporting multiples, we have updated the sample with these new detections by only updating the multiplicity information for the existing targets, without adding to that sample any new targets that may have been observed here. This sample multiplicity update does not substantially change the Vrijmoet et al. (2020) results. The threshold values of the four useful DR2 parameters may be lowered by ∼10% to select samples in which three out of four systems are unresolved multiples. The fifth criterion of missing DR2 entry or parallax remains valid. This consistency speaks to the robustness of the overall results of Vrijmoet et al. (2020).

6. Conclusions

In this work we have presented observations from the first 1.5 yr of our planned 3 yr speckle interferometry campaign at SOAR to observe M dwarfs within 25 pc. Key results to date include:

1. speckle measurements of 333 M dwarfs in 320 systems; 211 (63%) of these M dwarfs were resolved
2. four new orbits and one revised orbit with periods of 0.67–29 yr for M dwarfs with masses of 0.15–0.30 $M_{\odot}$
3. measurements of resolved companions for 76% of candidate multiples from Gaia DR2 identified by criteria for their astrometric fit parameters, as described in Vrijmoet et al. (2020).

Each observation reported here of a stellar companion is a step toward our goal of mapping the orbits of nearby M-dwarf multiples. Our project specifically targets M-dwarf systems with orbital periods of 0–30 yr and semimajor axes 0–6 au and the five orbits presented here span this full range, including some of the fastest-orbiting in our sample and some with the richest sets of similar observations in the literature. Many systems had already been observed at SOAR prior to this project and have measurements described in recent papers (e.g., Tokovinin et al. 2020, 2021). HRCam+SAM at SOAR has had many successful years observing stellar multiples (10 yr as of Tokovinin 2018b), and by focusing on the lowest-mass stars here we have thoroughly demonstrated its capabilities regarding faint, red systems.

Since the preparation of this paper began, with each observing run we have noted more systems that have enough data for orbit fits. This speckle program is thus well on its way to forming a significant contribution to the overall project of mapping M-dwarf orbits, and we anticipate continued success in the remaining 1.5 yr of this program. A future publication at the conclusion of this campaign will include several times the number of orbits presented here.

This project is an effort bringing together several observing methods, and as such demonstrates the power of these methods to complement and inform each other. Long-term ground-based astrometry from RECONS provides many full orbits and highlights systems with anomalous motion (but not necessarily distinguishable orbits) for speckle follow-up. The speckle interferometry from SOAR confirms or constrains those systems, and also efficiently captures the equal-mass systems that are not easily detectable via unresolved astrometry. Speckle observations may be combined with other resolutions in the literature, e.g., from adaptive optics, allowing orbits to be observed and characterized over long time baselines.

A multimethod approach is essential to this project, as the spatial scales involved in binary star formation and dynamical evolution span orders of magnitude in astronomical units. The

complex mix of physics may depend on several fundamental properties such as mass, system mass ratio, and age, making it imperative that a wide range of orbits be considered to make meaningful comparison between models and observations. Ultimately, the multiples reported here have far-reaching potential consequences for M-dwarf multiplicity, star formation, and local Galaxy mass distribution. This is because M dwarfs dominate the Galactic population, accounting for three out of every four stars (Henry et al. 2006, 2018). It is therefore essential to use all of the observing techniques at our disposal to determine not only which systems have companions, but to measure accurate sizes and shapes for their orbits, as those clues will reveal how the systems formed.

Colleagues at the Southern Astrophysical Research (SOAR) Telescope, the Cerro Tololo Inter-American Observatory (CTIO), and the SMARTS Consortium and have made this work possible.

This work has made use of data from the European Space Agency (ESA) mission Gaia (https://www.cosmos.esa.int/gaia), processed by the Gaia Data Processing and Analysis Consortium (DPAC, https://www.cosmos.esa.int/web/gaia/dpac/consortium). Funding for the DPAC has been provided by national institutions, in particular the institutions participating in the Gaia Multilateral Agreement.

This research has made use of the Washington Double Star Catalog maintained at the U.S. Naval Observatory.

The National Science Foundation has been consistently supportive of this effort under grants AST-0507711, AST-0908402, AST-1109445, AST-141206, AST-1715551, and AST-2108373.

Facilities: CTIO:0.9 m, CTIO:SOAR.

Appendix
Systems Worthy of Note

Here we describe several systems for which these SOAR results add significant new information or shed light on unusual observational histories. They are listed in order of ascending R. A., with WDS coordinate designations given in parentheses. The RECONS astrometry program mentioned for many systems refers to the long-term effort at the SMARTS 0.9 m.

1. SCR 0128-1458 AB (01287−1458): Through four resolutions at SOAR, we have confirmed the presence of this companion first noted tentatively in RECONS astrometry residuals by Riedel et al. (2018). The ΔI of 2.6–2.7 mag indicates the companion has mass $\lesssim$0.2 $M_{\odot}$. Continuing observations will provide valuable future constraints for the photocentric orbit in the RECONS astrometry, which is still incomplete after 10 yr of data.
2. LEHPM 1-1882 AB (01477−4836): Winters et al. (2017) revealed this binary via RECONS astrometry residuals. Its period is long, with the orbit not yet complete in what is now 15 yr of data. Although Winters et al. (2017) suggested the secondary companion contributes little light in R band, our three SOAR resolutions at I indicate a stellar companion with luminosity similar to the primary.
3. LHS 1561 AB (03347−0451): Seven SOAR observations over 2018.8–2020.9 have resolved this system's secondary to have moved 20° through its orbit. Jeffers et al. (2018) reported this system to be a spectroscopic triple; the tertiary is presumably less luminous and/or more closely bound to the primary, as our observed component's motion and ΔI indicate that we are consistently resolving the same (secondary) companion.
4. LHS 1582 AB (03434−0934): This system's 5 yr photocentric orbit was fully characterized in Vrijmoet et al. (2020), but the companion was not detected in our two SOAR observations. Comparison of the photometric (13 pc) and trigonometric (20 pc) distances by Riedel et al. (2010) and Lurie et al. (2014) indicated that the companion contributes noticeable light to the system. The limiting ΔI values of 1.4 mag at 0.″15 and 4.3 mag at 1.″0 from SOAR suggest it has mass $\lesssim$0.15 $M_{\odot}$.
5. GJ 1068 (04105−5336): Two observations of this target revealed a relatively closely separated background star; at 2019.6136 its separation and position angle were 3.″7177 and 38.°6, and at 2020.1111 they were 5.″1628 and 35.°5. Comparison with archival images from the CTIO/SMARTS 0.9 m confirm that this background star is not bound to GJ 1068. This target's results are thus not included in Table 2.
6. SCR 0702-6102 AB (07028−6103): We identified this system's companion early in the SOAR program as a fast mover, and have resolved it seven times from 2019.86–2020.99. The companion creates a low-amplitude perturbation in the RECONS astrometry residuals (as noted in Winters et al. 2017) with a period of ∼2.5 yr. That motion is consistent with what we have observed in the SOAR data.
7. SCR 0723-8015 AB (07240−8015): This system's color and absolute magnitude are consistent with a ∼0.1 $M_{\odot}$ star, and the clear perturbation indicates an orbital period that has not yet wrapped in 17 yr of RECONS astrometry data. The companion has not been detected in three observations in I at SOAR to limits of $\Delta I = 1.6$ and 3.0 at 0.″15 and 1.″0, respectively, indicating that it is of very low mass. This implies that the companion is a very low-luminosity red or white dwarf, or a brown dwarf.
8. SCR 0838-5855 AB (08380−5856): The RECONS astrometry indicates a large perturbation first shown in Winters et al. (2017) that now exceeds 50 mas in both R. A. and decl. directions, but has not wrapped in 14 yr of coverage. The two new SOAR resolutions are the first ever for this system and indicate the companion has $M_I = 14.6$, placing it very near end of the main sequence with a mass $\lesssim$0.1 $M_{\odot}$.
9. LHS 2071 AB (08553−2352): This system was first noted as binary by Riedel et al. (2010), who presented a preliminary fit to the partially observed orbit in RECONS astrometry data. Ten additional years of data have revealed the orbital period to be greater than the 21 yr of coverage to date. The four SOAR observations show clear orbital motion from 2018.2 to 2020.8; these will allow us to constrain the incomplete photocentric orbit in future work. The consistent ΔI of 2.4–2.6 mag indicate the companion has mass $\lesssim$0.2 $M_{\odot}$, but it is not substellar.
10. LP 788-001 AB (09314−1718): Winters et al. (2017) showed clear orbital motion for this system in the RECONS astrometry residuals, and noted that the companion must contribute little flux in I band. The orbit has not wrapped after 8 yr of coverage, and our SOAR observation in I did not reveal the companion. Because the absolute magnitude of this system sets the

primary mass at ∼0.1 $M_{\odot}$, the detection limits suggest that the companion is substellar.

11. LP 848-050 AB (10427−2416): This system exhibits an ∼8 yr orbit in the RECONS astrometry with a large-amplitude photocentric perturbation (see Figure 8 of Winters et al. 2017). Because the color and absolute magnitude of the system are consistent with a ∼0.1 $M_{\odot}$ star, the two nonresolutions at SOAR suggest that the companion is either a very-low-luminosity red or white dwarf, or a brown dwarf.
12. L 327-121 AB (12336−4826): The RECONS astrometric perturbation for this system shown in Winters et al. (2017) has continued in recent data now spanning 10 yr. This is likely the reason this system has a poor fit in Gaia DR2 and no parallax given in EDR3. The orbital period is ∼9 yr, and a robust fit of this orbit will be possible in future work, enabling dynamical masses to be determined by combining that fit with these three new SOAR resolutions. Winters et al. (2017) noted an excessive mismatch between photometric and trigonometric distance, suggesting either that the system is young or includes a third luminous component. The SOAR data indicate M_I values of 8.43 and 8.83 for the two components, implying masses of 0.4–0.5 $M_{\odot}$ and 0.3–0.4 $M_{\odot}$. The mass sum is consistent with the orbital information available, indicating that a third luminous component is unlikely.
13. LTT 6288 (15457−4330): This system's photocentric orbit was first described in Winters et al. (2017) and later updated in Vrijmoet et al. (2020). The orbital period is 9.9 yr. The two resolutions at SOAR indicate the companion's luminosity is consistent with mass $\lesssim$0.2 $M_{\odot}$, with the primary roughly twice as massive. The reliable RECONS astrometric orbit and continuing SOAR observations will enable a precise dynamical mass determination for both components in future work.
14. SCR 1546-5534 AB (15467−5535): The orbit shown in Henry et al. (2018) has continued in now 9 yr of RECONS astrometry, with preliminary fits suggesting an orbital period of ∼7 yr. The two SOAR resolutions reveal the companion to be somewhat less massive than the primary star, with the secondary's absolute I magnitude consistent with $\lesssim$ 0.1 $M_{\odot}$ and the primary's consistent with roughly twice that mass. The secondary is more likely stellar than substellar, however, as Henry et al. (2018) pointed out overluminosity evident in the ∼30% difference between photometric (7 pc) and trigonometric (10 pc) distances for this system.
15. LHS 3117 AB (15474−1054): Zechmeister et al. (2009) noted a radial velocity trend in VLT+UVES (Ultraviolet and Visible Spectrometer) data over ∼500 days starting in 2004, and noted this system as SB1. This signal was confirmed by the reanalysis of the same data by Tuomi et al. (2014). Our three new observations at SOAR over 2019.5–2020.2 reveal the companion, and the ΔI of 0.8–1.0 mag indicates it is likely a low-mass star rather than a brown dwarf.
16. GJ 1212 AB (17137−0825): This system has been noted as a spectroscopic binary by Reiners et al. (2012), Houdebine & Mullan (2015), and Jeffers et al. (2018). No relative positions have been published before our SOAR observations. These three resolutions show component B moving quickly around A from 2019.5 to 2020.2, sweeping through 191° in position angle. Estimating the orbital semimajor axis to be 1–3 times the maximum displacement seen so far and assuming mass sums of 0.5–0.7 $M_{\odot}$ yields orbital periods of 0.97–5.9 yr. This target is thus high priority for continued observations and orbit characterization on our SOAR program.
17. G 154-043 AB (18036−1859): Revealed as binary via the astrometric perturbation shown in (Winters et al. 2017), 10 yr of RECONS data now show this system to have an orbital period of 8–12 yr. The two observations at SOAR indicate that this binary has components with $M_I = 10.57$ and 11.92, implying masses of 0.15 $M_{\odot}$ and 0.12 $M_{\odot}$. The SOAR data also show significant motion through 27°, so future work should allow for a refined orbit and reliable masses.
18. LTT 7434 AB (18460−2856): As highlighted in Winters et al. (2017), this system has historically been challenging to interpret. The trigonometric distance is 1.4 times the photometric distance, implying two equal-mass components, yet the strong astrometric perturbation is only possible with unequal-mass components. Additional RECONS astrometry data acquired since Winters et al. (2017) continues the perturbation shown there, with the orbital period now estimated to be more than 20 yr. At SOAR we have twice resolved a companion at 0.″35–0.″39 (2019.61–2020.77) that is 1.4 mag fainter than the primary in I band; these are the first resolutions of this system. Bonfils et al. (2013) noted that this system is an SB2 with variable line width, suggesting the possibility of a close third component that could explain the excess flux. We will continue monitoring the long-term astrometry to complete the orbit and to look for any additional perturbations from a potential third companion.
19. GJ 829 AB (21296+1739): Delfosse et al. (1999) first reported this system to be binary and characterized its spectroscopic orbit. It was reported as visually resolved by Oppenheimer et al. (2001) at Palomar and by Dieterich et al. (2012) with HST/NICMOS, but in both cases no details of the resolutions are given. Our SOAR observations of the companion at 25.0–36.7 mas separations are the most detailed to date. The close separation of this system presents a challenge for HRCam+SAM to resolve consistently, but its 53 days orbital period (Delfosse et al. 1999) give us ample future opportunities to attempt observations. When we have observed the entire orbit visually, fitting that data will yield the orbital inclination, which we will combine with the Delfosse et al. (1999) spectroscopic fit to obtain the individual component masses.
20. LHS 3739 BC (21588−3226, a.k.a. LHS 3738 AB): The A-BC separation is 113″, forming a hierarchical triple. Riedel et al. (2010) first announced the companion to B based on RECONS astrometry and noted no significant overluminosity, indicating a much lower-mass companion. Lurie et al. (2014) presented an updated photocentric orbit; the six additional years of RECONS astrometry since then are consistent with that result. The BC pair has not been resolved at SOAR in two attempts, with limits of $\Delta I = 2.3$ at 0.″15 and 3.4 at 1.″0, implying a companion with mass lower than ∼0.1 $M_{\odot}$.

21. LEHPM 1-4771 (22302−5345): Although this binary's orbital motion was shown in Winters et al. (2017) and its orbit fit updated in Vrijmoet et al. (2020), the five SOAR observations reported here represent the first resolutions of the pair. The magnitude difference of $\Delta I = 0.9$–1.2 mag indicates a secondary somewhat less massive than the primary, consistent with the assertion in Winters et al. (2017) that the secondary must contribute little flux in the *R* band. Once more of the ∼6 yr orbit is covered with SOAR observations, we will combine the photocentric fit with SOAR resolutions to determine dynamical masses for the components.
22. LTT 9084 AB (22351−4218): This system was first resolved by Karmakar et al. (2020) in 2013 July, who found the binary to be separated by 398–405 mas with position angle 333°–334°, and brightness differences of <0.2 mag in each of *JHK* bands. Our SOAR observations yield $\Delta I = 0.0$, consistent with the near-infrared values. Thus, the components are likely of similar mass. Our observations spanning 2019.5–2020.8 show the secondary moving from 428 to 401 mas, to nearly the same separation as observed in 2013 by Karmakar et al. (2020). The position angles we observed, however, were 17°–21° greater than the 2013 observations, increasing through 2019.5–2020.8. This displacement suggests the companion passed through due north in the 6 yr between 2013 and 2019. Together, the available data suggest the orbit is either highly inclined or highly eccentric. Although the orbit is likely several decades in duration, continued observations over the next two years could rule out one of the above scenarios through any variations in the secondary's speed.

ORCID iDs

Eliot Halley Vrijmoet https://orcid.org/0000-0002-1864-6120
Andrei Tokovinin https://orcid.org/0000-0002-2084-0782
Todd J. Henry https://orcid.org/0000-0002-9061-2865
Jennifer G. Winters https://orcid.org/0000-0001-6031-9513
Elliott Horch https://orcid.org/0000-0003-2159-1463
Wei-Chun Jao https://orcid.org/0000-0003-0193-2187

References

Andrade, M. 2007, RMxAA, 43, 237
Baroch, D., Morales, J. C., Ribas, I., et al. 2018, A&A, 619, A32
Bate, M. R. 2015, in ASP Conf. Ser. 496, Living Together: Planets, Host Stars and Binaries, ed. S. M. Rucinski, G. Torres, & M. Zejda (San Francisco, CA: ASP), 37
Benedict, G. F., Henry, T. J., Franz, O. G., et al. 2016, AJ, 152, 141
Bergfors, C., Brandner, W., Janson, M., et al. 2010, A&A, 520, A54
Beuzit, J.-L., Ségransan, D., Forveille, T., et al. 2004, A&A, 425, 997
Bidelman, W. P. 1985, ApJS, 59, 197
Bonfils, X., Delfosse, X., Udry, S., et al. 2013, A&A, 549, A109
Bonnell, I. A., & Bate, M. R. 1994, MNRAS, 269, L45
Bowler, B. P., Cochran, W. D., Endl, M., et al. 2021, AJ, 161, 106
Bowler, B. P., Liu, M. C., Shkolnik, E. L., et al. 2015, ApJS, 216, 7
Brandt, T. D. 2021, ApJS, 254, 42
Brandt, T. D., Dupuy, T. J., & Bowler, B. P. 2019, AJ, 158, 140
Burgasser, A. J., Melis, C., Todd, J., et al. 2015, AJ, 150, 180
Calissendorff, P., Janson, M., Köhler, R., et al. 2017, A&A, 604, A82
Currie, T., Brandt, T. D., Kuzuhara, M., et al. 2020, ApJL, 904, L25
Cutri, R. M., Skrutskie, M. F., van Dyk, S., et al. 2003, yCat, II/246
Dahn, C. C., Harrington, R. S., Kallarakal, V. V., et al. 1988, AJ, 95, 237
Delfosse, X., Forveille, T., Beuzit, J.-L., et al. 1999, A&A, 344, 897
Dieterich, S. B., Henry, T. J., Golimowski, D. A., et al. 2012, AJ, 144, 64
Dieterich, S. B., Weinberger, A. J., Boss, A. P., et al. 2018, ApJ, 865, 28
Dittmann, J. A., Irwin, J. M., Charbonneau, D., et al. 2014, ApJ, 784, 156
Docobo, J. A., Gomez, J., Campo, P. P., et al. 2019, MNRAS, 482, 4096
Duchêne, G., & Kraus, A. 2013, ARA&A, 51, 269
Dupuy, T. J., Forbrich, J., Rizzuto, A., et al. 2016, ApJ, 827, 23
Dupuy, T. J., & Liu, M. C. 2017, ApJS, 231, 15
Dupuy, T. J., Liu, M. C., Bowler, B. P., et al. 2010, ApJ, 721, 1725
Duquennoy, A., & Mayor, M. 1991, A&A, 500, 337
Forveille, T., Beuzit, J.-L., Delfosse, X., et al. 1999, A&A, 351, 619
Gaia Collaboration, Brown, A. G. A., Vallenari, A., et al. 2021, A&A, 649, A1
Gaia Collaboration, Brown, A. G. A., Vallenari, A., et al. 2018, A&A, 616, A1
Gaia Collaboration, Prusti, T., de Bruijne, J. H. J., et al. 2016, A&A, 595, A1
Hartkopf, W. I., Mason, B. D., & Worley, C. E. 2001, AJ, 122, 3472
Heintz, W. D. 1994, AJ, 108, 2338
Henden, A. A., Templeton, M., Terrell, D., et al. 2016, yCat, II/336
Henry, T. J., Jao, W.-C., Paredes, L. A., et al. 2021, AAS Meeting Abstracts, 237, 333.05
Henry, T. J., Jao, W.-C., Subasavage, J. P., et al. 2006, AJ, 132, 2360
Henry, T. J., Jao, W.-C., Winters, J. G., et al. 2018, AJ, 155, 265
Horch, E. P., van Altena, W. F., Demarque, P., et al. 2015, AJ, 149, 151
Houdebine, E. R., & Mullan, D. J. 2015, ApJ, 801, 106
Izmailov, I. S. 2019, AstL, 45, 30
Janson, M., Bergfors, C., Brandner, W., et al. 2014, ApJS, 214, 17
Janson, M., Hormuth, F., Bergfors, C., et al. 2012, ApJ, 754, 44
Jao, W.-C., Henry, T. J., Gies, D. R., et al. 2018, ApJL, 861, L11
Jao, W.-C., Henry, T. J., Subasavage, J. P., et al. 2003, AJ, 125, 332
Jao, W.-C., Henry, T. J., Subasavage, J. P., et al. 2005, AJ, 129, 1954
Jao, W.-C., Henry, T. J., Subasavage, J. P., et al. 2011, AJ, 141, 117
Jao, W.-C., Henry, T. J., Subasavage, J. P., et al. 2014, AJ, 147, 21
Jeffers, S. V., Schöfer, P., Lamert, A., et al. 2018, A&A, 614, A76
Jódar, E., Pérez-Garrido, A., Díaz-Sánchez, A., et al. 2013, MNRAS, 429, 859
Karmakar, S., Rajpurohit, A. S., Allard, F., et al. 2020, MNRAS, 498, 737
Kervella, P., Arenou, F., Mignard, F., et al. 2019, A&A, 623, A72
Kervella, P., Mérand, A., Ledoux, C., et al. 2016, A&A, 593, A127
Koen, C., Kilkenny, D., van Wyk, F., et al. 2010, MNRAS, 403, 1949
Köhler, R., Ratzka, T., & Leinert, C. 2012, A&A, 541, A29
Konopacky, Q. M., Ghez, A. M., Barman, T. S., et al. 2010, ApJ, 711, 1087
Kratter, K. M., Matzner, C. D., Krumholz, M. R., et al. 2010, ApJ, 708, 1585
Kroupa, P. 2008, The Cambridge N-Body Lectures (Berlin: Springer), 181
Kuffmeier, M., Calcutt, H., & Kristensen, L. E. 2019, A&A, 628, A112
Lee, A. T., Offner, S. S. R., Kratter, K. M., et al. 2019, ApJ, 887, 232
Lee, Y.-N., Offner, S. S. R., Hennebelle, P., et al. 2020, SSRv, 216, 70
Lurie, J. C., Henry, T. J., Jao, W.-C., et al. 2014, AJ, 148, 91
Mann, A. W., Dupuy, T., Kraus, A. L., et al. 2019, ApJ, 871, 63
Martín, E. L., Koresko, C. D., Kulkarni, S. R., et al. 2000, ApJL, 529, L37
Mason, B. D., Gies, D. R., Hartkopf, W. I., et al. 1998, AJ, 115, 821
Mason, B. D., Hartkopf, W. I., Miles, K. N., et al. 2018, AJ, 155, 215
Mason, B. D., Wycoff, G. L., Hartkopf, W. I., et al. 2001, AJ, 122, 3466
Moe, M., & Di Stefano, R. 2017, ApJS, 230, 15
Moe, M., Kratter, K. M., & Badenes, C. 2019, ApJ, 875, 61
Offner, S. S. R., Dunham, M. M., Lee, K. I., et al. 2016, ApJL, 827, L11
Oppenheimer, R., Golimowski, D. A., Kulkarni, S. R., et al. 2001, AJ, 121, 2189
Pringle, J. E. 1989, MNRAS, 239, 361
Raghavan, D., McAlister, H. A., Henry, T. J., et al. 2010, ApJS, 190, 1
Reiners, A., Joshi, N., & Goldman, B. 2012, AJ, 143, 93
Riedel, A. R., Finch, C. T., Henry, T. J., et al. 2014, AJ, 147, 85
Riedel, A. R., Silverstein, M. L., Henry, T. J., et al. 2018, AJ, 156, 49
Riedel, A. R., Subasavage, J. P., Finch, C. T., et al. 2010, AJ, 140, 897
Scardia, M., Prieur, J.-L., Pansecchi, L., et al. 2019, Inf. Circ, 198, 1
Ségransan, D., Delfosse, X., Forveille, T., et al. 2000, A&A, 364, 665
Shan, Y., Yee, J. C., Bowler, B. P., et al. 2017, ApJ, 846, 93
Söderhjelm, S. 1999, A&A, 341, 121
Tokovinin, A. 2016, Orbit: Idl Software For Visual, Spectroscopic, And Combined Orbits, Zenodo
Tokovinin, A. 2017, AJ, 154, 110
Tokovinin, A. 2018a, Inf. Circ, 194, 1
Tokovinin, A. 2018b, PASP, 130, 035002
Tokovinin, A. 2018c, Inf. Circ, 195, 1
Tokovinin, A. 2019, Inf. Circ, 199, 1
Tokovinin, A. 2020, Inf. Circ, 201, 1
Tokovinin, A., Cantarutti, R., Tighe, R., et al. 2016, PASP, 128, 125003
Tokovinin, A., Mason, B. D., & Hartkopf, W. I. 2010, AJ, 139, 743
Tokovinin, A., Mason, B. D., Hartkopf, W. I., et al. 2015, AJ, 150, 50
Tokovinin, A., Mason, B. D., Mendez, R. A., et al. 2019, AJ, 158, 48
Tokovinin, A., Mason, B. D., Mendez, R. A., et al. 2020, AJ, 160, 7
Tokovinin, A., Mason, B. D., Mendez, R. A., et al. 2021, AJ, 162, 41

Tuomi, M., Jones, H. R. A., Barnes, J. R., et al. 2014, MNRAS, 441, 1545
Udry, S., Mayor, M., Delfosse, X., et al. 2000, in IAU Symp. 200, Birth and Evolution of Binary Stars, ed. B. Reipurth & H. Zinnecker (Cambridge: Cambridge Univ. Press), 158
van de Kamp, P. 1967, Principles of Astrometry (San Francisco, CA: Freeman)
van Leeuwen, F. 2007, A&A, 474, 653
Vrijmoet, E. H., Henry, T., Tokovinin, A., et al. 2021, AAS Meeting Abstracts, 237, 530.02
Vrijmoet, E. H., Henry, T. J., Jao, W.-C., & Dieterich, S. B. 2020, AJ, 160, 215
Ward-Duong, K., Patience, J., De Rosa, R. J., et al. 2015, MNRAS, 449, 2618
Weis, E. W. 1996, AJ, 112, 2300
Winters, J. G., Henry, T. J., Jao, W.-C., et al. 2019, AJ, 157, 216
Winters, J. G., Henry, T. J., Lurie, J. C., et al. 2015, AJ, 149, 5
Winters, J. G., Sevrinsky, R. A., Jao, W.-C., et al. 2017, AJ, 153, 14
Zechmeister, M., Kürster, M., & Endl, M. 2009, A&A, 505, 859
Zirm, H. 2003, IAUDS, 151, 1